

## Characterization of Photophysics and Mobility of Single Molecules in a Fluid Lipid Membrane

Th. Schmidt,\* G. J. Schütz, W. Baumgartner, H. J. Gruber, and H. Schindler

*Institute for Biophysics, University of Linz, Altenberger Strasse 69, 4040 Linz, Austria*

*Received: August 17, 1995*<sup>®</sup>

Properties of single fluorescence-labeled lipids in a fluid phospholipid membrane were analyzed using sensitive fluorescence microscopy. The high signal-to-noise ratio for detection of individual fluorescence-labeled molecules of 5–70 permitted detailed study of their photophysical parameters. From single fluorophores a signal of 49 counts/ms was detected when excited above their saturation intensity of 7.6 kW/cm<sup>2</sup>. These data, obtained at the level of individual fluorophores, are found to agree quantitatively with predictions from a conventional three-level model using known ensemble-averaged rate constants. Light-induced photochemistry of single fluorophores was found to occur as a sudden disappearance of their fluorescence characterized by a photobleaching efficiency of  $9 \times 10^{-6}$ . These photophysical properties of the fluorescence label permitted analysis of the motion of individual lipid molecules. Lipid motion was tracked at a rate of up to 66 images per second. The high fluorescence image-contrast allowed for determination of lipid positions with a precision of 30 nm. For short length-scales the observed trajectories were described by a random two-dimensional motion with a lateral diffusion constant of  $1.42 \times 10^{-8}$  cm<sup>2</sup>/s. Free diffusion was found to be restricted to length-scales of 100 nm, attributed to membrane defects.

### Introduction

In the last years techniques have been developed for detection and manipulation of single dye molecules or atoms in the gas, liquid, and solid phase. The trapping of single ions in electromagnetic fields made ultrahigh-resolution spectroscopy accessible, showing the finest details in atomic spectra.<sup>1</sup> High-resolution spectroscopy also allowed for identification of single fluorescent molecules in solids at low temperature<sup>2,3</sup> with applications to spectroscopy on single molecules in crystals and polymers.<sup>4,5</sup> The first imaging of single molecules was carried out at liquid-helium temperature using an intensified CCD-camera.<sup>6</sup> Single-molecule detection and spectroscopy in the liquid phase was stimulated by perspectives in analytical chemistry and bioscience. The early finding of Hirschfeld<sup>7</sup> that a single macromolecule can be detected when stained with  $\sim 100$  dye molecules has prompted efforts for the detection of monolabeled biomolecules and individual fluorophores in solvents. The techniques used are based on highly-sensitive confocal fluorescence microscopy in which the observed volume is reduced to  $<1$  pL. It was possible to detect single dye molecules in flowing streams,<sup>8</sup> droplets,<sup>9,10</sup> and levitated microdroplets.<sup>11</sup> Application of these techniques in analytical chemistry and bioscience has been extensively discussed.<sup>12</sup> The confocal arrangement was mainly focused on the detection of single molecules in small volumes, and only sophisticated analysis of the data permitted determination of spatial information such as diffusion constants.<sup>9,12</sup> In contrast, optical near-field microscopy made direct imaging of single molecules possible.<sup>13</sup> It reaches a spatial resolution of  $\sim 12$  nm and has been extended to spectroscopy on fluorescent dyes in polymer matrices or crystals<sup>14–16</sup> and photobiological membranes.<sup>17</sup> However, the time resolution of near-field microscopy is too low to follow dynamical processes like motion and redistribution of components in biological membranes. For biophysical characterization of individual component mobility, NANOVID-

microscopy (nanoparticle video microscopy)<sup>18</sup> has become a widespread technique.<sup>19–22</sup> It was designed to observe motion in biological systems with high spatial and time resolution. Detection of biomolecules was achieved either via binding of gold particles<sup>18,19,21</sup> or fluorescent latex spheres<sup>20</sup> or via heavy fluorescence labeling.<sup>7,22–24</sup> The time resolution is given by the video-frequency, and the positional accuracy is  $\sim 2$  nm, only limited by the signal-to-noise ratio.<sup>25</sup>

Very recently it has been shown that individual dye molecules could be imaged in an aqueous environment when immobilized on actin filaments.<sup>26</sup> In turn, we have shown that the time resolution for single-molecule imaging can be increased into the millisecond regime, which made possible the direct visualization of the diffusional trajectory of monolabeled lipid molecules for the first time.<sup>27</sup> Here, we employ this imaging technique for the determination of photophysical characteristics of single fluorophores covalently bound to lipids and for detailed examination of the two-dimensional mobility of individual lipids in a fluid lipid membrane. Unitary fluorescence intensity, fluorescence saturation, and photobleaching statistics of individual fluorophores are investigated, showing the perspectives and limits of microscopy on the single-molecule level.

### Experimental Section

**Sample Preparation.** Supported lipid bilayers of 1-palmitoyl-2-oleoyl-*sn*-glycero-3-phosphocholin (POPC, Avanti Polar Lipids) are transferred onto glass- and quartz-substrates by the Langmuir–Blodgett technique.<sup>28,29</sup> Fluorescent analogues of 1-palmitoyl-2-oleoyl-*sn*-glycero-3-phosphoethanolamine (POPE) were synthesized by derivatization with 5-(and 6-)carboxy-tetramethylrhodamine succinimidyl ester (TMR, Molecular Probes). Before usage, the substrates were cleaned in chromic acid for 30 min and extensively washed in bidistilled water. The lipids were spread at 23 °C from chloroform with a lipid content of 5 mg/mL at the air/buffer (100 mM NaCl, 10 mM NaH<sub>2</sub>PO<sub>4</sub>, pH 7.5) interface in a monolayer trough (Fromhertz-type, Mayer Feinttechnik, Göttingen, Germany) to a surface

\* To whom correspondence should be addressed.

<sup>®</sup> Abstract published in *Advance ACS Abstracts*, November 15, 1995.

pressure of 3 mN/m. After 2 min allowance for solvent evaporation the film was compressed to 32 mN/m. At the applied conditions, the monolayers were in the liquid-expanded phase. Monolayers were deposited onto the substrate at constant surface pressure. First a POPC-monolayer was deposited by vertically moving the substrate through the air/buffer interface at a velocity of 7.5 mm/min. Subsequently, this first monolayer was brought horizontally into contact with the second monolayer, containing unlabeled (POPC) and fluorescence-labeled (TMR/POPE) lipids in molar ratios between  $x = 6 \times 10^{-4}$  and  $x = 6 \times 10^{-9}$ . The coated substrate was pushed through the air/buffer interface and attached to an open quartz cuvette (136QS, Hellma). From the area reduction of the monolayers during the transfer steps a coverage of the substrate of 95–100%, on average, was calculated.

**Optical Setup.** The cuvette was mounted on an inverted microscope (Axiovert 135-TV, Zeiss) equipped with an  $M = 100\times$  objective (PlanNeofluar  $\times 100$ , NA = 1.3, Zeiss). In some experiments an additional  $1.6\times$ -magnification lens (Optovar, Zeiss) was used. Through the epiport of the microscope the sample was illuminated with the 514 nm line of an Ar<sup>+</sup>-laser (Innova 306, Coherent) running in TEM<sub>00</sub>-mode. The excitation light was circular polarized by means of a  $\lambda/4$ -plate. A 200 mm lens in front of the dichroic mirror defocused the laser-spot on the sample to a Gaussian profile with  $(6.1 \pm 0.8) \mu\text{m}$  full-width at half-maximum (fwhm). An acousto-optic modulator (1205C-1, Isomet) in combination with a function generator (Model 502SL, Exact) was used to provide exact timing of the illumination and as a variable attenuator. The fluorescence was monitored through a dichroic mirror (515DRLPEXT02, Omega) in combination with a band-pass (570DF70, Omega) and a low-pass filter (OG550–3mm, Schott) by a liquid-N<sub>2</sub> cooled slow-scan CCD-camera system (AT200, 16 bit, 40 kHz,  $1.6 \text{ e}^-/\text{count}$ , 4 counts/pixel readout noise, Photometrix) equipped with a Tek512CB/AR chip ( $A_{\text{pixel}} = 27 \times 27 \mu\text{m}^2$  pixel size, Tektronix). The total collection efficiency for the fluorescence of TMR-labeled lipids was  $\eta_{\text{det}} = (3 \pm 1)\%$ .

A test of the mechanical stability<sup>22</sup> of our apparatus was carried out by taking 200 images of two fluorescent latex-spheres (30 nm size, Molecular Probes) which were immobilized on a cover-slip. The distance of the two spheres was found to vary less than 10 nm during the 20 s time-scale of a typical experiment.

**Data Acquisition.** Data acquisition was performed on a 486-66 PC using software distributed with the camera (PMIS, Photometrix). Parts of the CCD-chip were covered by a mechanical shutter restricting illumination to a small region of the array (typically  $40 \times 40 \text{ pixel}^2$ , i.e.,  $10.8 \times 10.8 \mu\text{m}^2$  in the image-plane). By programming the hardware and by slight modification of the camera electronics, it was possible to vary the image repetition time with minimal values of 7 ms in a fast mode and minimal values of 70 ms in a slow continuous mode,<sup>30</sup> respectively. In the fast mode a sequence of up to 14 images can be taken depending on the illuminated area and the storage capacity of the CCD-chip, whereas the slow mode permits continuous imaging limited by computer memory only. Compared to NANOVID-microscopes, that are commonly equipped with an intensified CCD-camera having video-frequency capture rates, the apparatus described here is slower by a factor of 2 in the continuous slow mode and faster by a factor of 4 in the fast mode.

Before each acquisition cycle an image without laser illumination was taken from which the average dark counts were determined. This average dark-value was subtracted from every image in subsequent acquisitions.

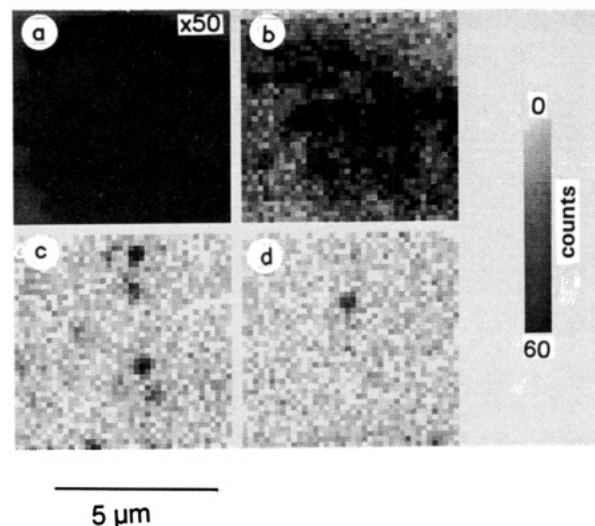


**Figure 1.** Images of  $6.8 \times 6.8 \mu\text{m}^2$  taken from supported lipid bilayers of POPC with different TMR/POPE content: (a)  $6.5 \times 10^{-3}$  mol/mol [TMR/POPE]/[POPC] (intensity divided by 50); (b)  $6.5 \times 10^{-6}$  mol/mol; (c)  $6.5 \times 10^{-8}$  mol/mol; (d)  $6.5 \times 10^{-9}$  mol/mol. The samples were illuminated with  $57 \pm 14 \text{ kW/cm}^2$  for 5 ms and imaged using  $M = 160\times$  optical magnification. Images are scaled between 0 (white) and 60 counts/pixel (black).

**Data Analysis.** Data were analyzed using a software-package<sup>31</sup> written in MATLAB (MathWorks). In brief, first the images were filtered using a Gaussian correlation-filter.<sup>32</sup> A threshold criterion which was determined from the image noise yielded starting values for a nonlinear fitting procedure of two-dimensional Gaussian profiles to the original images.<sup>33</sup>  $\chi^2$ , exponential, and F tests,<sup>34</sup> applied to the fitting results, yielded an unbiased criterion for the acceptance of individual fluorescence peaks. In this way the position of each molecule was found with 30 nm precision,<sup>25,32</sup> and its fluorescence intensity was determined with an uncertainty of <20%. The Gaussian peaks had a width of  $1.5 \pm 0.4$  pixels (fwhm) reflecting the point-transfer-function of the microscope optics as measured from images of 30 nm fluorescent-beads. The determination of molecule positions was used to analyze their motion from the positional shifts in successive images. The two-dimensional trajectory or 'trace' of the molecule within the lipid membrane was obtained using a Vogel-algorithm.<sup>31</sup> The mean-square-displacement for each molecule was calculated from such trajectories for every time-lag.<sup>21</sup>

## Results and Discussion

**Fluorescence Intensity of Single Fluorophores Predicted from High-Concentration Data.** Figure 1 presents typical fluorescence images of POPC-membranes observed for different molar ratios,  $x$ , of TMR-labeled POPE to unlabeled POPC covering the range between  $6.5 \times 10^{-9}$  and  $6.5 \times 10^{-4}$  mol/mol. The scaling of the images is chosen between 0 (white) and 60 counts/pixel (black). The fluorescence intensity in Figure 1a was divided by a factor of 50 with respect to those of Figures 1b–d. The images show areas of  $6.8 \times 6.8 \mu\text{m}^2$  of lipid membranes illuminated for 5 ms by a Gaussian-shaped laser beam with  $d_L = 6.1 \pm 0.8 \mu\text{m}$  full-width at half-maximum (fwhm). We define here the average excitation intensity,  $I_L$ , as the total power measured at the sample divided by the fwhm-area,  $\pi(d_L/2)^2 = 29 \pm 5 \mu\text{m}^2$ , of the laser spot. For the images in Figure 1,  $I_L = 57 \text{ kW/cm}^2$ . At the highest TMR/POPE concentration ( $x = 6.5 \times 10^{-4}$  mol/mol, Figure 1a) the fluorescence intensity follows smoothly that of the laser intensity with little spatial variation. Variations increase with decreasing

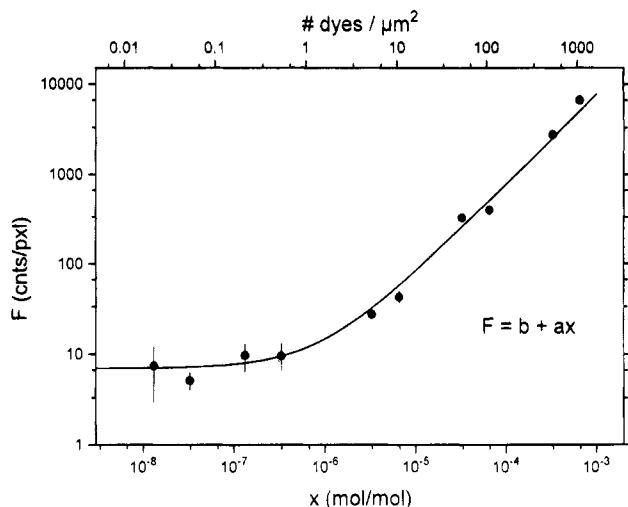


**Figure 2.** Average fluorescence intensity,  $F$ , for a  $2 \times 2 \mu\text{m}^2$  image-area of a lipid membrane as a function of the molar ratio of [TMR/POPE]/[POPE],  $x$ , in the top layer. The samples were illuminated for 5 ms with a laser intensity of  $57 \pm 14 \text{ kW/cm}^2$  and imaged using  $M = 160\times$  optical magnification. The average fluorescence intensity follows a linear dependence with  $x$  yielding a background of  $b = 7 \pm 2$  counts/pixel and a slope of  $a = 7.8 \pm 0.7 \times 10^6$  counts/pixel (solid line).

fluorophore concentration ( $x = 6.5 \times 10^{-6} \text{ mol/mol}$ , Figure 1b) until well resolved single fluorescence spots are recognized at  $x = 6.5 \times 10^{-8}$  (Figure 1c) and  $x = 6.5 \times 10^{-9} \text{ mol/mol}$  (Figure 1d). For complete unlabeled membranes no fluorescence spots were found (not shown). As shown in ref 27, these fluorescence spots can be identified as images of individual fluorescence-labeled lipid molecules.

The fluorescence intensity of a single fluorescent molecule can be predicted from such high concentration images. For this, the mean fluorescence intensity,  $F$ , determined in an area within the fwhm-disk of the illumination spot was measured for  $x$  between  $6.5 \times 10^{-9}$  and  $6.5 \times 10^{-4} \text{ mol/mol}$ . The result is shown in double-logarithmic form in Figure 2. The samples were illuminated for 5 ms with  $I_L = 57 \text{ kW/cm}^2$ . The solid line represents a linear fit to the data with  $F = b + ax$ . A background intensity  $b = 7 \pm 2$  counts/pixel and a linear increase with a slope  $a = (7.8 \pm 0.7) \times 10^6$  counts/pixel are found. The linear increase of  $F$  with molar ratio implies that no concentration quenching due to aggregation of the fluorophores occurs, at least not up to  $x = 6 \times 10^{-4} \text{ mol/mol}$ . From the slope of  $F$  on  $x$  the intensity due to an individual fluorescent molecule,  $\bar{F}_{sm}$ , can be predicted: Assuming a mean-area per lipid of  $A_{lipid} = 63 \text{ \AA}^2$  in a supported lipid bilayer,<sup>35</sup> the intensity per fluorescence-labeled lipid is  $\bar{F}_{sm} = aM^2A_{lipid}/A_{pixel} = 172 \pm 15$  counts/molecule for the magnification  $M = 160$  used.

**Fluorescence Intensity of Individual Fluorophores.** At low concentrations of fluorescence-labeled lipid the fluorescence intensity of individual fluorophores was determined (see Data Analysis). Distributions of the fluorescence intensity of all identified fluorophores,  $F_{sm,i}$ , in typically 120 images of an experiment are shown in Figure 3 for three different laser intensities (Figure 3a) and illumination times (Figure 3b). The data are presented in the form of probability-density-functions,  $\rho(F_{sm})$ , calculated by<sup>34</sup>

$$\rho(F_{sm}) = \frac{1}{\sqrt{2\pi} N} \sum_{i=1}^N \frac{1}{dF_{sm,i}} \exp\left(-\frac{(F_{sm} - F_{sm,i})^2}{2dF_{sm,i}^2}\right) \quad (1)$$

with fluorescence intensities  $F_{sm,i}$  and respective confidence intervals  $dF_{sm,i}$ , derived from the nonlinear least-square fitting

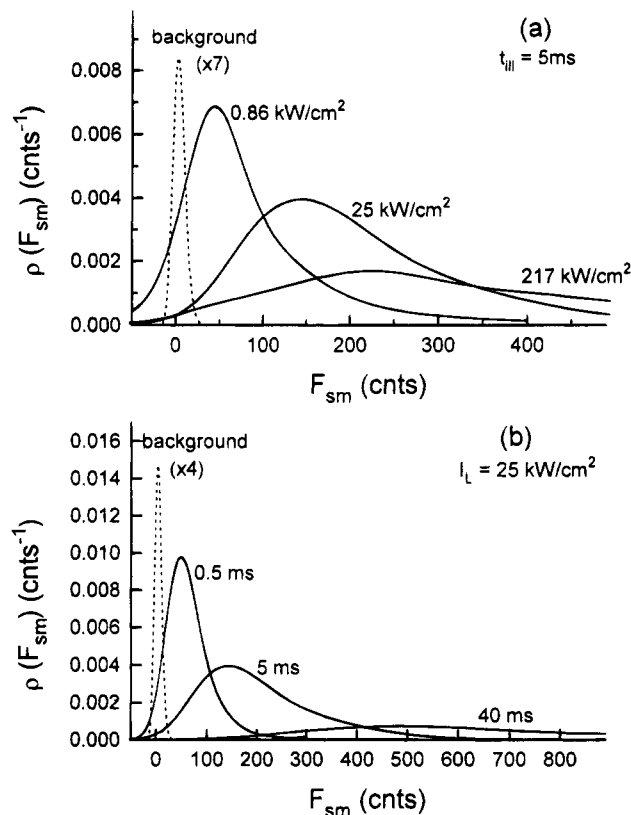


**Figure 3.** Probability density,  $\rho(F_{sm})$ , of the fluorescence intensity obtained for individual fluorescence-labeled lipids. The probability density of the background intensity is shown for comparison (dashed). (a)  $\rho(F_{sm})$  for  $I_L = 0.86 \pm 0.22$ ,  $25 \pm 6$ , and  $217 \pm 54 \text{ kW/cm}^2$  at constant  $t_{ill} = 5 \text{ ms}$ .  $N = 26$ ,  $342$ , and  $129$  fluorophore molecules were analyzed. The most probable values are  $\bar{F}_{sm} = 41$ ,  $149$ , and  $237$  counts, respectively. (b)  $\rho(F_{sm})$  for  $t_{ill} = 0.5$ ,  $5$ , and  $40 \text{ ms}$  at constant  $I_L = 25 \pm 6 \text{ kW/cm}^2$ .  $N = 12$ ,  $342$ , and  $265$  fluorophores were analyzed. The most probable values are  $\bar{F}_{sm} = 45$ ,  $149$ , and  $493$  counts, respectively.

procedure.<sup>34</sup> The mean fluorescence intensity of individual fluorescence-labeled lipids,  $\bar{F}_{sm}$ , as determined from the position of the maximum of  $\rho(F_{sm})$  is calculated from such distributions. For  $I_L = 57 \text{ kW/cm}^2$  and  $t_{ill} = 5 \text{ ms}$ ,  $\bar{F}_{sm} = 173 \pm 20$  counts is found (not shown, see Figure 4a). This value is in excellent agreement with the value of  $\bar{F}_{sm} = 172$  counts predicted from Figure 2, which provided the same evidence,<sup>27</sup> that the isolated fluorescence peaks observed can be identified with individual TMR molecules.

The mean fluorescence intensity determined from individual TMR/POPE molecules,  $\bar{F}_{sm}$ , shows a typical saturation behavior as seen in Figure 4. At constant  $t_{ill} = 5 \text{ ms}$ , shown in Figure 4a,  $\bar{F}_{sm}$  increases with  $I_L$  up to  $\sim 25 \text{ kW/cm}^2$  and turns over into a saturation value of  $F_\infty = 246$  counts at higher laser intensities. Contrarily, at fixed  $I_L = 25 \text{ kW/cm}^2$ , shown in Figure 4b,  $\bar{F}_{sm}$  increases monotonously with  $t_{ill}$  up to a value of  $1520$  counts at  $t_{ill} = 150 \text{ ms}$ . Both observations can be explained quantitatively by a three-state model.

**Three-Level Saturation.** Saturation of the fluorescence with laser intensity can be explained considering the energy-level structure of the fluorescent molecule as illustrated in Figure 5. A conventional four-level model of the fluorophore including a ground- ( $n_G$ ), singlet-excited- ( $n_S$ ), triplet-excited- ( $n_T$ ), and photoproduct-state ( $n_P$ ) coupled with the appropriate rate-constants is assumed. In a first step the reaction-pathway to the photoproduct state is neglected ( $k_b = 0$ ). In such a three-state model the variation of the fluorescence with illumination

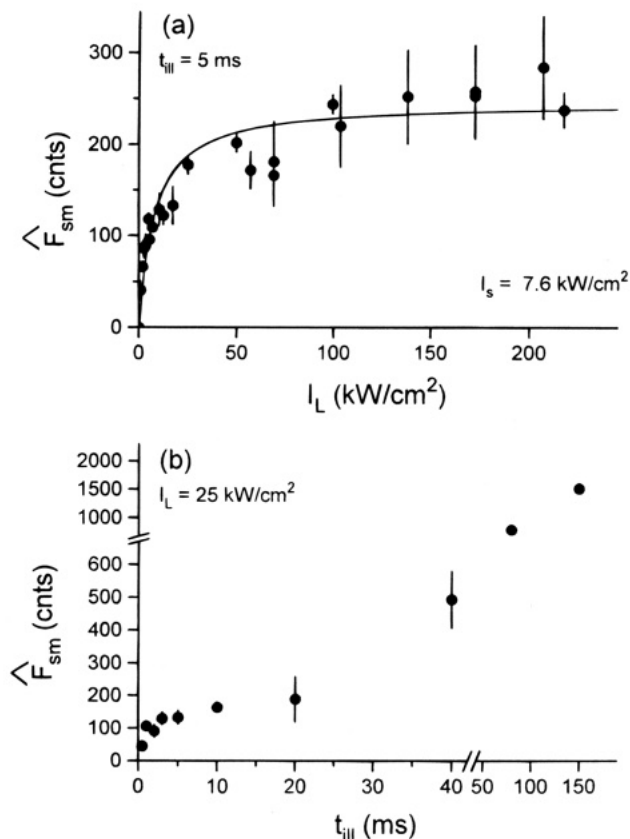


**Figure 4.** Single molecule fluorescence intensity,  $\hat{F}_{sm}$ , as a function of (a) laser intensity,  $I_L$ , at constant illumination time,  $t_{ill} = 5$  ms, and (b) illumination time at constant  $I_L = 25 \pm 6$  kW/cm<sup>2</sup>. The solid line in part a represents a fit to  $\hat{F}_{sm} = k_{\infty} t_{ill} / (1 + I_s / I_L)$  with  $k_{\infty} = 49 \pm 3$  counts/ms and saturation intensity  $I_s = 7.6 \pm 1.1$  kW/cm<sup>2</sup>.

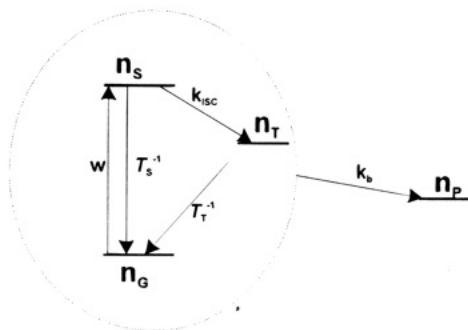


**Figure 5.** Energy-level diagram of a tetramethylrhodamine (TMR) molecule.

intensity and time is given by  $F_{sm} = k_{\infty} t_{ill} / (1 + I_s / I_L)$ ,<sup>9,36</sup> with saturation intensity,  $I_s$ , and  $k_{\infty}$ ,

$$I_s = \frac{hc}{3\lambda_L \sigma_0} \frac{\frac{1}{\tau_s} + k_{isc}}{1 + k_{isc} \tau_T} \quad (2)$$

$$k_{\infty} = \frac{\eta_{det} \Phi}{\tau_s (1 + k_{isc} \tau_T)}$$

In eq 2  $\tau_s$  and  $\tau_T$  represent the lifetimes of the excited singlet- and triplet-state, respectively,  $k_{isc}$  is the intersystem crossing rate,  $\lambda_L$  is the wavelength of excitation,  $\sigma_0 = 1.9 \times 10^{-16}$  cm<sup>2</sup> is the mean absorption cross-section for randomly oriented fluorophores,  $\Phi = 0.28$  is the quantum efficiency of TMR in water,<sup>37,38</sup> and  $\eta_{det} = (3 \pm 1)\%$  is the detection efficiency of the apparatus used. For derivation of eq 2 the circular

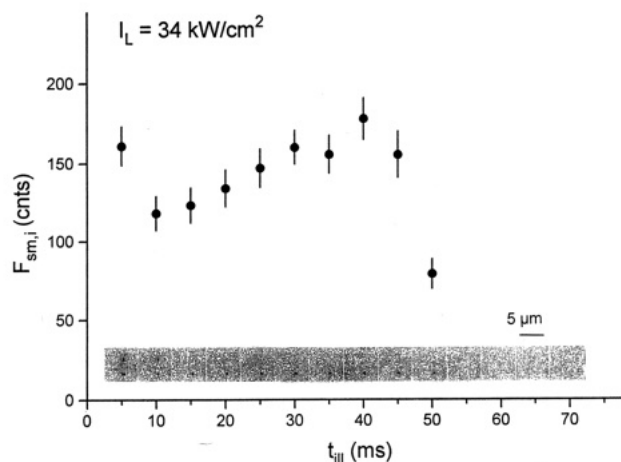


**Figure 6.** Fluorescence intensity variation of an individual fluorescence-labeled lipid illuminated consecutively every 30 ms with  $I_L = 34 \pm 9$  kW/cm<sup>2</sup> and  $t_{ill} = 5$  ms. The original images showing a  $6.8 \times 6.8 \mu\text{m}^2$  membrane area are displayed in parallel. The sudden disappearance of one molecule after the 10th image is observed.

polarization of the laser-beam and the parallel direction of the transition dipole moment of the fluorophore with respect to the membrane-surface<sup>39</sup> are taken into account. A fit of the data in Figure 4a yields  $k_{\infty} = 49 \pm 3$  counts/ms and  $I_s = 7.6 \pm 1.1$  kW/cm<sup>2</sup> (solid line in Figure 4a).

All rate constants involved in the model of Figure 5 have been measured for rhodamine molecules in various samples. For  $\tau_s = 2.1$  ns of TMR in water,<sup>38</sup>  $\tau_T = 2 \mu\text{s}$  of a rhodamine dye (Rh6G) in water,<sup>40</sup> and  $k_{isc} = 0.03\tau_s^{-1}$ ,<sup>37</sup>  $I_s = 11$  kW/cm<sup>2</sup> and  $k_{\infty} = 135 \pm 45$  counts/ms are derived from eq 2. The saturation intensity found experimentally is in very good agreement with the theoretical value. This is further confirmed by measurements at high TMR/POPE concentrations ( $x = 6 \times 10^{-4}$  mol/mol) in which  $I_s = 5.7 \pm 1.6$  kW/cm<sup>2</sup> was obtained.<sup>30</sup> The value for  $k_{\infty}$  determined experimentally is smaller by a factor of three compared to that determined from the three-level model. In order to explain this discrepancy, one has to keep in mind that the involved rate constants, in particular, the intersystem crossing rates, and the fluorescence quantum yield are extremely sensitive to the environment,<sup>37,38</sup> making such *ab-initio* determination difficult. However, the reasonable agreement between the experimental and theoretical values further supports the identification of the isolated fluorescence peaks with individual fluorescence-labeled lipids given in ref 27.

As expected from the model  $\hat{F}_{sm}$  varies linearly with illumination time for fixed laser intensity, as seen in Figure 4b for  $t_{ill} \leq 5$  ms. The decrease of the slope in  $\hat{F}_{sm}$  with illumination time for  $t_{ill} > 5$  ms is a manifestation of light-induced photochemistry.

**Light-Induced Photochemistry.** Individually observed fluorophores undergo light-induced photochemistry as seen in Figure 6. In this image sequence obtained for  $I_L = 34$  kW/cm<sup>2</sup>,  $t_{ill} = 5$  ms, and 30 ms delay between successive images, a single fluorescence-labeled lipid can be identified, which suddenly disappears after the 10th image, being exposed to the excitation light for 50 ms. In all experiments performed these disappearances occurred as a one-step process within our time resolution. We attribute this, as in ref 15, to light-induced bleaching of the fluorophore. To elucidate the statistics of this process, the accumulated illumination time for individual fluorophores before bleaching occurs is evaluated, as seen in the inset of Figure 7. From the histogram taken from experiments at  $I_L = 17$  kW/cm<sup>2</sup> the average photobleaching time  $\tau_B = 11.5 \pm 2.5$  ms



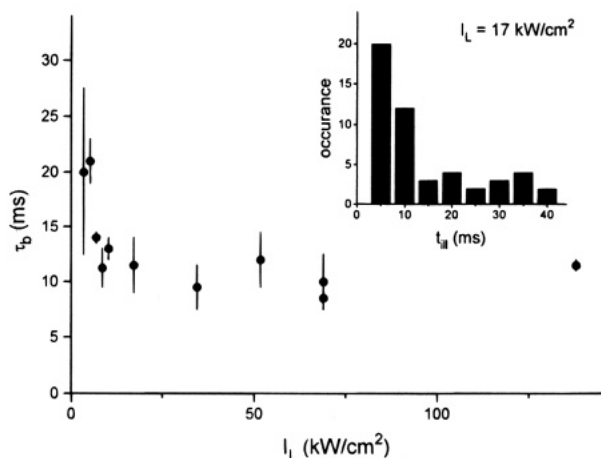


**Figure 7.** Average bleaching time,  $\tau_b$ , of individual TMR/POPE molecules as a function of the laser intensity,  $I_L$ . Inset: Histogram of accumulated illumination time for individual fluorophores before bleaching occurred when illuminated with  $I_L = 17 \pm 4$  kW/cm<sup>2</sup>. An average bleaching time  $\tau_b = 11.5 \pm 2.5$  ms is determined from a monoexponential fit to the data.

was estimated by approaching the histogram with a monoexponential decay. Such analysis was performed for various laser intensities, as shown in Figure 7. With increasing  $I_L$  the photobleaching time drops from  $\tau_b = 20$  ms at  $I_L = 2$  kW/cm<sup>2</sup> to  $\tau_b = 7$  ms for  $I_L > 50$  kW/cm<sup>2</sup>. The dependence of  $\tau_b$  on  $I_L$  shows that the effect of bleaching is due to a light-induced process included in the four-level model of Figure 5. From the data shown in Figure 7 the photobleaching efficiency,  $\Phi_b = \tau_s/\tau_b^\infty(1 + k_{isc}\tau_T) = 9 \times 10^{-6}$ , is obtained using the saturation-limited value of  $\tau_b^\infty = 7$  ms. The value of  $\Phi_b$  is in good agreement with the value we obtained for high-concentration samples ( $\Phi_b = 5 \times 10^{-6}$ )<sup>30</sup> and values measured for rhodamine molecules on silica surfaces<sup>41</sup> and those embedded in a polymer matrix,<sup>15</sup> for which photobleaching efficiencies between  $10^{-7}$  and  $10^{-5}$  were reported.

At low laser intensities we observed that parts of the molecules bleached very rapidly, while others had considerably longer lifetimes and were observed for the whole image sequence (see inset of Figure 7). This observation of a bimodal photobleaching behavior was also reported for individual fluorophores embedded in polymer matrices.<sup>42</sup> Multiexponential bleaching of the fluorophores has also been observed for samples at high fluorophore concentrations.<sup>43</sup> Although a large amount of experimental and theoretical work has been done, the photophysics of the bleaching process is still not known in full detail.<sup>37,43</sup> Observations on the level of individual molecules, as presented here, are expected to yield new and more detailed information on photobleaching. In particular, processes like excimer formation, for which both excitation of the fluorophore and its mobility play a role, might be directly visualized.

**Signal-to-Noise Ratio for Single Molecule Detection.** In order to calculate the fluorescence-background statistics, a sample with no fluorescence-labeled lipid was prepared and its intensity distribution calculated (dashed lines in Figure 3). The distribution of the background intensity did not change within the range of the illumination parameters used throughout Figure 3. The Gaussian-shaped distribution is essentially due to readout noise of the CCD-camera and has a width of  $\sigma_b = 7$  counts.

For application of the technique discussed here, it is important to quantify the reliability for identification of a single molecule in the sample. Individual molecules can be detected as long as their fluorescence intensity is distinguishable from the background. Thus, the signal-to-noise ratio for detecting a single

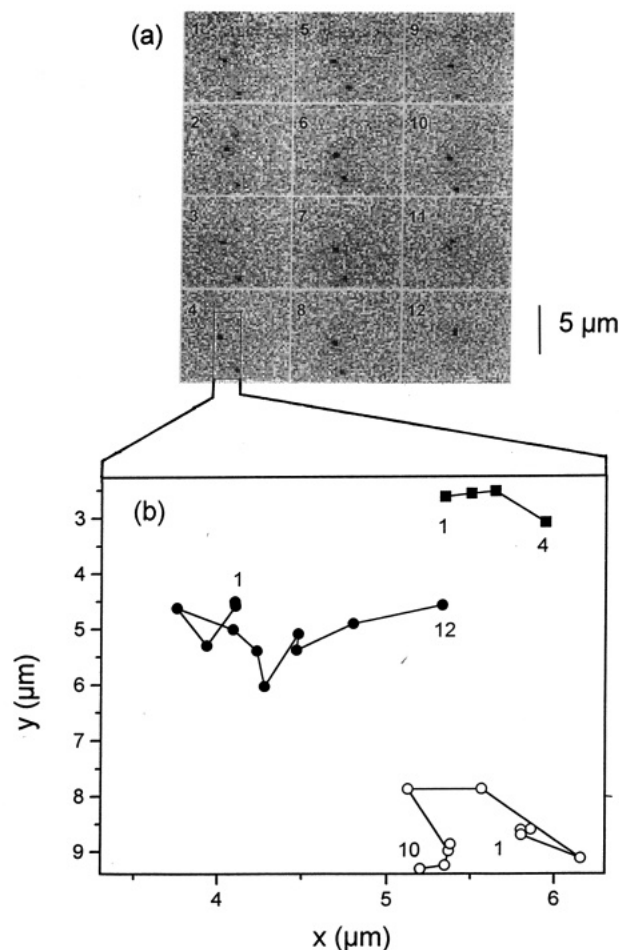


**Figure 8.** (a) 12 images of  $12.2 \times 9.5 \mu\text{m}^2$  taken from a fluid lipid membrane of  $x = 10^{-8}$  mol/mol. Three individual fluorescence-labeled lipids were identified. The images were taken every 10 ms using an illumination time of 5 ms and a laser intensity of  $57 \pm 14$  kW/cm<sup>2</sup>. (b) Trajectories of the three molecules identified in the image sequence of Figure 8a.

fluorophore is defined by  $S/N = \hat{F}_{sm}/\sigma_b$ . For  $I_L = 0.86$  kW/cm<sup>2</sup> and  $t_{ill} = 5$  ms the signal-to-noise ratio is  $S/N = 5$  and increases up to  $S/N = 70$  for  $I_L = 25$  kW/cm<sup>2</sup> and  $t_{ill} = 40$  ms. The high  $S/N$  for  $t_{ill}$  in the millisecond range at modest laser intensities shows the perspectives of the method used. Molecular recognition and diffusion processes studied in bioscience occur on millisecond timescales; thus, they are expected to be accessible with the apparatus used.

**Two-Dimensional Diffusion.** Lipids undergo motion within the fluid lipid membrane, as is apparent from the images in Figure 8a. A series of 12 images of a  $12.2 \times 9.5 \mu\text{m}^2$  area of a POPC-membrane doped with TMR/POPE at  $x = 10^{-8}$  mol/mol is shown. The images were taken repetitively every 10 ms at  $I_L = 57$  kW/cm<sup>2</sup> and  $t_{ill} = 5$  ms. Three fluorescence-labeled lipid molecules were observed, and their respective trajectories are presented in Figure 8b. The high signal-to-noise ratio permitted us to track individual molecules with a positional accuracy of 30 nm, which is  $\sim 1/8$ th of the diffraction limit. From these positional data the mean-square-displacement, MSD, was calculated for all time-lags,  $t_{lag}$ .<sup>21</sup>

$$\text{MSD}(t_{lag}) = \frac{1}{\sum_{t_i - t_j = t_{lag}}} \sum_{t_i - t_j = t_{lag}} (\vec{r}(t_i) - \vec{r}(t_j))^2 \quad (3)$$

In eq 3  $\vec{r}(t)$  represents the position of the molecule at time  $t$ . Assuming a two-dimensional diffusion of the lipids within the

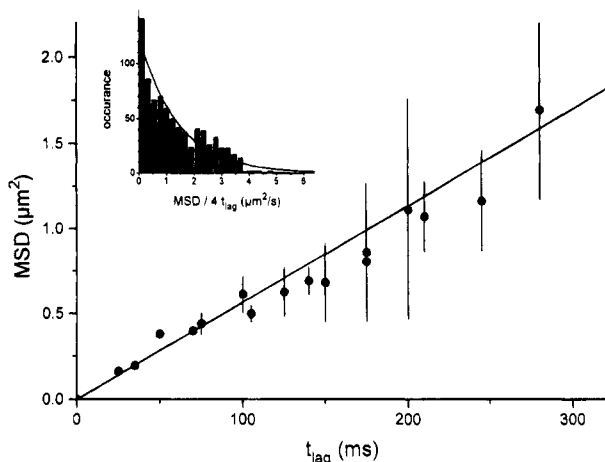


**Figure 9.** Ensemble average of the mean-square-displacement, MSD, as a function of time-lag,  $t_{\text{lag}}$ , obtained from 531 single-molecule trajectories. The solid line represents a fit according to  $\text{MSD} = 4\langle D_{\text{lat}} \rangle t_{\text{lag}}$ . A mean two-dimensional lateral diffusion constant  $\langle D_{\text{lat}} \rangle = (1.42 \pm 0.23) \times 10^{-8} \text{ cm}^2/\text{s}$  is obtained. Inset: Histogram of values for  $\text{MSD}/4t_{\text{lag}}$  as calculated from single-molecule trajectories. The exponential decay with increasing  $\text{MSD}/4t_{\text{lag}}$  is characterized by  $\langle D_{\text{lat}} \rangle = (1.4 \pm 0.3) \times 10^{-8} \text{ cm}^2/\text{s}$  (solid line).

membrane, the lateral diffusion constant,  $D_{\text{lat}}$ , is given by  $\text{MSD}(t_{\text{lag}}) = 4D_{\text{lat}}t_{\text{lag}}$ .<sup>44</sup> The result of an analysis of 531 trajectories of individual TMR/POPE molecules is shown in Figure 9. As expected for Brownian motion, a linear increase of MSD with  $t_{\text{lag}}$  is found for the ensemble average with  $\langle D_{\text{lat}} \rangle = (1.42 \pm 0.23) \times 10^{-8} \text{ cm}^2/\text{s}$ . A statistical analysis of the value of  $\text{MSD}/4t_{\text{lag}}$  is given in the inset of Figure 9. The exponential decay with increasing  $\text{MSD}/4t_{\text{lag}}$  (solid line) also resembles that expected for a random walk model characterized by  $\langle D_{\text{lat}} \rangle$ .<sup>44</sup> Photobleaching experiments<sup>45</sup> using samples at high concentration in our laboratory, however, revealed  $D_{\text{lat}} = (0.77 \pm 0.13) \times 10^{-8} \text{ cm}^2/\text{s}$ ,<sup>30</sup> which is smaller by a factor of two compared to the  $\langle D_{\text{lat}} \rangle$  value found for individual lipid molecules. We attribute this difference to the influence of the experimental length-scales of the two methods. While the length-scale in photobleaching experiments is several micrometers, the length-scale of the present experiments is  $\sim 100 \text{ nm}$ . It is known that lipid membranes are inhomogeneous on a length-scale of  $\sim 100 \text{ nm}$ ,<sup>46,47</sup> which in turn is manifested by a diffusion constant which varies with the method used.<sup>20,48</sup>

We were able to directly detect the effect of such inhomogeneities of a membrane on the lipid diffusion by single-molecule microscopy as shown in Figure 10. In a particular membrane the lateral diffusion constant was  $D_{\text{lat}} = 1.08 \times 10^{-8} \text{ cm}^2/\text{s}$  for short time-lags decreasing to  $D_{\text{lat}} = 0.64 \times 10^{-8} \text{ cm}^2/\text{s}$  for  $t_{\text{lag}} > 140 \text{ ms}$ . This observation is interpreted by us as the result of an island structure of the membrane surrounded by barriers for lipid diffusion. Within one island, at short time-lags, the diffusion is fast, whereas crossing the barrier is a slower process causing the decrease of  $D_{\text{lat}}$  for longer time-lags. The average size of the islands is  $\sim 400 \text{ nm}$ , as estimated from the region of  $t_{\text{lag}}$  in which the higher  $D_{\text{lat}}$  value is observed. This experiment shows one of the advantages of single molecule observation, which allows for detection of small inhomogeneities of the sample, an issue often occurring in bioscience.

**Further Systems Studied.** Experiments were further performed on two other systems: Lipids derivatized with the fluorescent molecule fluorescein could be detected with the same signal-to-noise ratio as reported here for rhodamine-labeled lipids. The diffusion behavior was equivalent, but as expected, the photobleaching efficiency was  $\sim 10$  times higher than that of the rhodamine-labeled lipid.<sup>49</sup> Further, isocyanine molecules

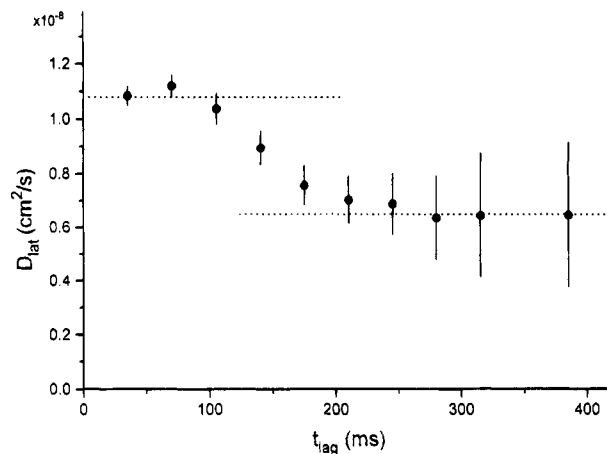


**Figure 10.** Variation of the lateral diffusion constant,  $D_{\text{lat}}$ , with time-lag,  $t_{\text{lag}}$ , in an inhomogeneous lipid membrane. Fourteen different areas on the sample were analyzed.

embedded in a polymer-matrix<sup>50</sup> could be detected with higher fluorescence yield compared to that in the lipid systems. We think that the higher fluorescence yield is probably due to a lower intersystem-crossing rate of the molecule in the polymer-matrix and to a higher fluorescence quantum-yield of unbound to lipid- or peptide-bound molecules.<sup>37</sup> We found  $\sim 1$  isocyanine molecule per  $\mu\text{m}^2$  in this sample, which excellently agrees with the density found by near-field microscopy.<sup>50</sup>

Currently, we are investigating a system in which a single antigen-antibody reaction might be observed in a phospholipid membrane. We have already shown that a monolabeled antibody linked to a lipid could be observed and that its diffusion constant is reduced by a factor of two with respect to that of lipids.<sup>51</sup>

## Summary and Conclusions

State-of-the-art imaging techniques allowed for determination of photophysical characteristics of individual fluorescence molecules in a fluid lipid membrane. Millisecond dynamics at extremely small surface densities, which is a typical problem in surface science and membrane biophysics, could be directly visualized. It is envisioned that such studies on the single-molecule level will provide new insights into the behavior and function of biomolecules with least interference, since only a single fluorescence label is necessary for detection.

**Acknowledgment.** We thank P. Hinterdorfer for enlightening discussions on diffusion and fluorescence in lipid membranes and T. Haselgrübler for kindly providing us with the fluorescence-labeled lipids. This work was supported by the Austrian Research Fund project S06607-MED and the Austrian Ministry for Research and Development.

## References and Notes

- (1) For recent reviews see: *Advances in Atomic, Molecular and Optical Physics*; Bates, D., Benderson, B., Eds. Academic Press: San Diego, 1993; Vol. 31, and references therein.
- (2) Kador, L.; Horne, D. E.; Moerner, W. E. *Phys. Rev. Lett.* **1989**, *62*, 2535.
- (3) Orrit, M.; Bernard, J. *Phys. Rev. Lett.* **1990**, *65*, 2716.
- (4) For a review see: Moerner, W. E.; Basché, Th. *Angew. Chem., Int. Ed. Engl.* **1993**, *32*, 457. Moerner, W. E. *Science* **1994**, *265*, 46.
- (5) Köhler, J.; Disselhorst, A. J.; Donckers, M. C. J.; Groenen, E. J.; Schmidt, J.; Moerner, W. E. *Nature* **1993**, *363*, 242. Wachtrup, J.; von Borczyskowski, C.; Bernard, J.; Orrit, M.; Brown, R. *Nature* **1993**, *363*, 244.

- (6) Güttler, F.; Irmgartinger, T.; Plakhotnik, T.; Renn, A.; Wild, U. P. *Chem. Phys. Lett.* **1994**, 217, 393. Moerner, W. E.; Plakhotnik, T.; Irmgartinger, T.; Croci, M.; Palm, V.; Wild, U. W. *J. Phys. Chem.* **1994**, 98, 7382.
- (7) Hirschfeld, T. *Appl. Opt.* **1976**, 15, 2965.
- (8) Shera, E. B.; Seitzinger, N. K.; Davis, L. M.; Keller, R. A.; Soper, S. A. *Chem. Phys. Lett.* **1990**, 174, 553.
- (9) Nie, S.; Chiu, D. T.; Zare, R. N. *Science* **1994**, 266, 1018.
- (10) Rigler, R.; Widengren, J.; Mets, Ü. In *Fluorescence Spectroscopy*; Wolfbeis, O., Ed.; Springer: Berlin, 1992.
- (11) Whitten, W. B.; Ramsey, J. M.; Arnold, S.; Bronk, B. V. *Anal. Chem.* **1991**, 63, 1027.
- (12) Eigen, M.; Rigler, R. *Proc. Natl. Acad. Sci. U.S.A.* **1994**, 91, 5740.
- (13) Betzig, E.; Chichester, R. J. *Science* **1993**, 262, 1422.
- (14) Trautman, J. K.; Macklin, J. J.; Brus, L. E.; Betzig, E. *Nature* **1994**, 369, 40.
- (15) Ambrose, W. P.; Goodwin, P. M.; Martin, J. C.; Keller, R. A. *Phys. Rev. Lett.* **1994**, 72, 160.
- (16) Xie, X. S.; Dunn, R. C. *Science* **1994**, 265, 361.
- (17) Dunn, R. C.; Holtom, G. R.; Mets, L.; Xie, X. S. *J. Phys. Chem.* **1994**, 98, 3094.
- (18) Geerts, H.; de Brabanter, M.; Nydens, R.; Geuens, S.; Moeremans, M.; de Mey, J.; Hollenbeck, P. *Biophys. J.* **1987**, 52, 775.
- (19) Quian, H.; Sheetz, M. P.; Elson, E. L. *Biophys. J.* **1993**, 60, 910.
- (20) Fein, M.; Unkeless, J.; Chuang, F. Y. S.; Sassaroli, M.; da Costa, R.; Väänänen, H.; Eisinger, J. J. *Membr. Biol.* **1993**, 135, 83.
- (21) Kusumi, A.; Sako, Y.; Yamamoto, M. *Biophys. J.* **1993**, 65, 2021.
- (22) Ghosh, R. N.; Webb, W. W. *Biophys. J.* **1994**, 66, 1301.
- (23) Peck, K.; Stryer, L.; Glazer, A. N.; Mathies, R. A. *Proc. Natl. Acad. Sci. U.S.A.* **1989**, 86, 4087.
- (24) Käs, J.; Strey, H.; Sackmann, E. *Nature* **1994**, 368, 648.
- (25) Bobroff, N. *Rev. Sci. Instr.* **1986**, 57, 1152.
- (26) Funatsu, T.; Harara, Y.; Tokunaga, M.; Saito, K.; Yanagida, T. *Nature* **1995**, 374, 555.
- (27) Schmidt, Th.; Schütz, G. J.; Gruber, H. J.; Schindler, H. Submitted to *Proc. Natl. Acad. Sci. U.S.A.*
- (28) Blodgett, K. B. *J. Am. Chem. Soc.* **1935**, 57, 1007.
- (29) Tamm, L. K.; McConnell, H. M. *Biophys. J.* **1985**, 47, 105.
- (30) Schütz, G. J. Master thesis, University of Linz, 1995.
- (31) Baumgartner, W. Master thesis, University of Linz, 1995.
- (32) Gelles, J.; Schnapp, B. J.; Sheetz, M. P. *Nature* **1988**, 331, 450.
- (33) Marquard, D. W. *J. Soc. Ind. Appl. Math.* **1963**, 11, 431.
- (34) Bevington, P. R.; Robinson, D. K. *Data Reduction and Error Analysis for the Physical Sciences*; McGraw Hill: New York, 1992.
- (35) Selig, J. In *Physical Properties of Model Membranes and Biological Membranes*; Balian, R., Ed.; North Holland: Amsterdam, 1981.
- (36) Demtröder, W. *Laser Spectroscopy*; Springer Series in Chemical Physics, Vol. 5; Springer: Berlin, 1988.
- (37) Tsien, R. Y.; Waggoner, A. In *Handbook of Biological Confocal Microscopy*; Pawley, J. B., Ed.; Plenum Press: New York, 1990.
- (38) Soper, S. A.; Nutter, H. L.; Keller, R. A.; Lloyd, D. M.; Shera, E. B. *Photochem. Photobiol.* **1993**, 57, 972.
- (39) Lieberherr, M.; Fattinger, Ch.; Lukosz, W. *Surf. Sci.* **1987**, 189, 664.
- (40) Windengren, J.; Rigler, R.; Mets, Ü. *J. Fluoresc.* **1994**, 4, 255.
- (41) Huston, A. L.; Reimann, C. T. *Chem. Phys.* **1991**, 149, 401.
- (42) Meixner, A. J.; Zeisel, D.; Bopp, M. A.; Tarrach, G. *Opt. Eng.*, in press.
- (43) Song, L.; Hennink, E. J.; Young, I. T.; Tanke, H. J. *Biophys. J.* **1995**, 68, 2586.
- (44) Chandrasekhar, S. *Rev. Mod. Phys.* **1943**, 15, 1.
- (45) Tsay, T. T.; Jacobson, K. A. *Biophys. J.* **1991**, 60, 360.
- (46) Chi, L. F.; Anders, M.; Fuchs, H.; Johnston, R. R.; Ringsdorf, H. *Science* **1993**, 259, 213.
- (47) Hui, S. W.; Viswanathan, R.; Zasadzinski, Z. A.; Israelachvili, J. N. *Biophys. J.* **1995**, 68, 171.
- (48) Saxton, M. J. *Biophys. J.* **1993**, 64, 1766.
- (49) Haugland, R. P. *Handbook of Fluorescent Probes and Research Chemicals*; Molecular Probes: Eugene, 1992.
- (50) A sample of 1,1'-dioctadecyl-3,3',3'-tetramethylindocarbocyanine (diI) in a poly(methyl methacrylate) film was a kind gift of J. K. Trautman, AT&T Bell Laboratories, Murray Hill, NJ.
- (51) Schmidt, Th.; Schütz, G. J.; Gruber, H. J.; Schindler, H. In preparation.

JP952440W